Journal of Metals, Materials and Minerals, Vol.20 No.2 pp.53-61, 2010

Effect of Sintering on Microstructure and Properties of Hydroxyapatite Produced by Different Synthesizing Methods

Naruporn MONMATURAPOJ* and Chokchai YATONGCHAI

National Metal and Materials Technology Center, 114 Thailand Science Park, Paholyothin Road, Pathumthani 12120, Thailand

Abstract

The aim of this study is to investigate the effect of the sintering schedule on microstructure and properties of hydroxyapatite which is produced by different synthesizing methods. Hence, wet-chemical precipitation and solid-state reaction were performed to prepare nano-sized hydroxyapatite (HA) powders. Powders were then uniaxially pressed and sintered by varying temperatures and times. XRD and SEM were used to identify phases and morphology. Density and porosity of the sintered sample were determined using the Archimedes technique. Flexural strength was measured by a universal testing machine. The results show that density and strength could be improved by increasing the sintering temperature in both HAW and HAD. However, with increasing sintering temperatures, average grain sizes of HAW and HAD samples were not significantly increased. The sintering temperature seems to play a more important role than sintering time in the densification process of hydroxyapatite. In addition, the thermal stability in sintered HAD samples induced a weaker flexural strength of samples in comparison with HAW. Therefore, the optimized microstructure and properties of sintered hydroxyapatite can be prepared by using the suitable synthesizing method together with the workable sintering schedule for each synthesizing process.

Key words: Hydroxyapatite, Microstructures, Mechanical properties, Bioceramics

Introduction

Hydroxyapatite ($Ca_{10}(PO_4)_6(OH)_2$, regularly known as HA, is a calcium phosphate based compound. It possesses excellent osteoconductivity and bioactivity because the chemical composition is similar to the mineral in bones and teeth.[1-2] However, due to its poor mechanical properties(Tracy & Doremus, 1984), use of the material is restricted for load bearing clinical applications. Consequently, several processes for synthesizing HA powders have been developed over the past decades including wet synthesis(Jarcho & Bolen, 1976; Liu et al., 2001; Santos et al., 2004; Zhang & Gonsalves, 1997; Afshar et al., 2003 and García et al., 2005), solid-state reaction(Arita et al., 1995 and Kim et al., 2000) and hydrothermal(Zhang & Vecchio, 2007 and Zhu et al., 2008) methods, etc. The initial purpose of these processes is to produce HA powders in desired characteristics, for example a high specific surface area, fine particle size and size distribution with small particle agglomeration. Another purpose is to improve the mechanical properties of sintered HA.[14] A number of investigations suggested that nano-sized HA encourages superior bioactivity than coarser particles.[15] All of these properties of HA powders depend on which process is performed. Due to a high homogeneous purity of precipitated powders, the precipitation method is used in particular, and also most commonly. It is simple to be operated and does not require any special equipment.[16-17] The solid-state reaction method, meanwhile, is simple, high productive and not too expensive. It is therefore a valuable alternative to commercially produce HA powders for industry.[10]

Many investigations(Akao et al., 1981 and Martin & Brown, 1995) reported on the sintering process in order to improve mechanical properties of HA ceramics. However, they varied only the sintering temperature. There is no interesting report on sintering time. In addition, information about the compared sinterability of HA synthesized by these two methods is limited. Therefore, to produce nanocrystalline HA powders, conventional wet-chemical precipitation was performed in this work as well as a solid-state reaction. The microstructure and properties of HA prepared from the powders sintered by varying both temperatures and times will be discussed and evaluated in this paper.

*Corresponding author Tel: +66 2564 6500 ext. 4437; Fax: +66 2564 6446; E-mail: narupork@mtec.or.th

Materials and Experimental Procedures

Preparation of HA Powders

Nano-sized hydroxyapatite powders were produced by two different synthesizing methods:

Method 1: Hydroxyapatite was prepared by using the conventional wet-chemical precipitation method. $Ca(NO_3)_2.4H_2O$ and $(NH_4)_2HPO_4$ were dissolved in deionized water separately; then each solution was stirred for 2 minutes until each starting material was completely dissolved. The pH of each aqueous solution was adjusted to 11 by using NH_4OH solution 25%. $Ca(NO_3)_2$ aqueous solution was added drop-wise. The solution was vigorously stirred $(NH_4)_2HPO_4$ at room temperature for about 1 hour in order to produce a milky solution. The gelatinous precipitate was then stirred for one further hour. After that the reflux process was employed at 100°C for 1 hour followed by aging for 24 hours. It was then washed and filtered in a filter glass with application of a mild suction. After filtration, the compact, sticky, filter cake was dried overnight at 80°C. After drying the as-dried samples were crushed by using mortar and pestle.

Method 2: In this method, hydroxyapatite was synthesized by a solid-state reaction method. $CaCO_3$ and $CaHPO_4$ as starting powders were mixed and ball milled with zirconia balls for 48 hours by using deionized water as a medium. After milling, the slurry was dried overnight at 100°C.

In the text, the two synthesized powders described above will be referred to as HAW and HAD, respectively.

A mixture of polyvinyl alcohol (1wt%, PVA) as a binder and polyethylene glycol (2wt%, PEG) as a plasticizer was added to HAW and HAD powders. The ready mixed HAW and HAD powders were compacted under a stress of 2 MPa. The green bodies of HAW and HAD were sintered at temperatures of 1200°C and 1250°C for 1, 2 and 4 hours in a furnace. All the sintered specimens were then polished to a 3 μm prior to the evaluation.

Characterization

Specific surface area of the as-synthesized powders was determined by the nitrogen absorption analysis (BET: Autosorb-1C, Quantachrome instrument). Phase analysis was carried out on the as-synthesized powders and sintered specimens by using X-ray diffractometer **(**XRD**:** JEOL JDX 3530). It was operated from 10°-70° 2θ at a scan speed of 2° 2θ/min and a step size of 0.02° 2θ with $Cu_{K\alpha}$ radiation (λ_{Cu} = 0.1540562 nm) at 50 kV and 30 mA. The spectra were analyzed by using JADE software and JCPDS cards. The morphology of the as-synthesized powders and sintered samples was investigated by scanning electron microscopy (SEM: JEOL 6301F). The particle sizes of as-synthesized powders and grain sizes with different sintering temperatures and times were determined by using the linear intercept method. At least 150 grains were measured to obtain the average value.

Density and Mechanical Testing

The density of the sintered compact disks (13 mm x 5 mm) was determined by using the Archimedes technique in deionized water. The result was derived from the average of five measurements for each sintering temperature and time.

The flexural strength of the sintered specimens was performed on a bar with the dimensions 4 mm x 3 mm x 30 mm (after polishing dimension). A three-point bending was tested by using a universal testing machine (Instron 55R4502) at a crosshead speed of 0.5 mm/min. The equation for calculating the flexural strength is

$$\sigma = 3PL/2bd^2$$

Where

P is the load required to break the specimen,
L is the span (the distance between the outer supports, L = 20 mm),
b is the specimen width,
and d is the thickness.[20]

There were five specimens prepared for each condition of which the average value of flexural strength was taken. The mean flexural strength was reported with the standard deviation of each data set.

Results and Discussion

Powder Characteristics

The specific surface areas of 110.35 and 46.98 m^2/g can be prepared through the as-synthesized HAW and HAD powders, respectively. This difference might be due to the different synthesizing routes. The higher specific surface area of HAW could be associated to the smaller

particle size with respect to that of HAD as shown by SEM images in Figure 1(a) and (b). However, to avoid undesirable agglomerates that can be formed if powders with higher surface area were selected, a low specific surface area of HAD powder might be suitable for sintering.[21]

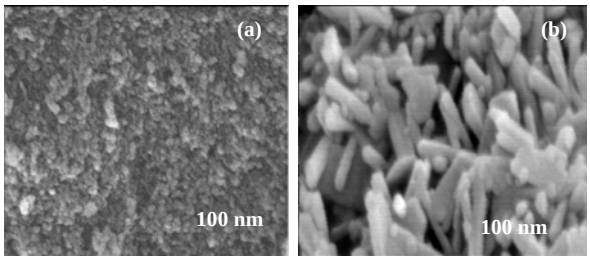

Figure 1. SEM images of as-synthesized powders (a) HAW and (b) HAD.

Figure 1(a) and (b) are SEM images show the microstructures of the as-synthesized HAW and HAD powders, respectively. The micrograph of HAW powder sample presents very fine and irregular particles in the nanometer size range (~10 nm). The SEM image of HAD powder also depicts a nano-size particle but with rod-like shape of an aspect ratio of about 3 (~50 nm width x ~150 nm length). The nano-particle observed by SEM micrographs correlated well with the BET results.

Figure 2 shows XRD patterns of the as-synthesized HAW and HAD powders. The XRD patterns can index only peaks corresponding to hydroxyapatite, JCPDS no. 09-0432 of HAW and HAD powders. No secondary phase such as tricalcium phosphate (TCP) or calcium oxide appeared. The broadening peak of the crystalline HA can be referred to the nano-size of hydroxyapatie powders produced by these two methods.

Effect of Sintering Temperature and Time on Phase Formation of Sintered Samples

Figure 3(a) and (b) display the XRD patterns of the sintered HAW samples at 1200°C and 1250°C for 1, 2 and 4 hours. At 1200°C, HA started to decompose because peaks that were due to β-TCP and α-TCP were observed after sintering for 1 hour. These peaks were retained as a minor phase in the higher sintering times as shown in Figure 3(a). At 1250°C, only peaks corresponding to HA crystal can be indexed in the samples after sintering for all periods of time, shown in Figure 3(b). For these samples, the intensity of HA crystal peaks was not significantly increased by increasing sintering time. It seems that the sintering time showed a less pronounced effect on the crystallinity of the HA sample. Meanwhile, the sintering temperature played a considerable role in the phase formation of hydroxyapatite.

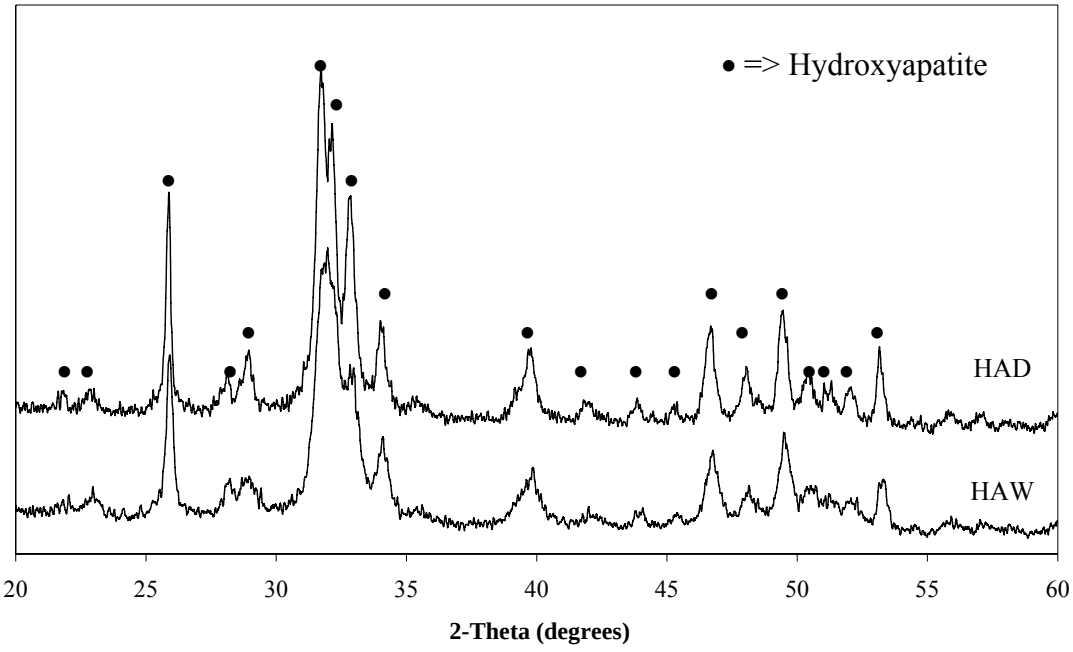

Figure 2. XRD Patterns of as-dried HAW and HAD powders.

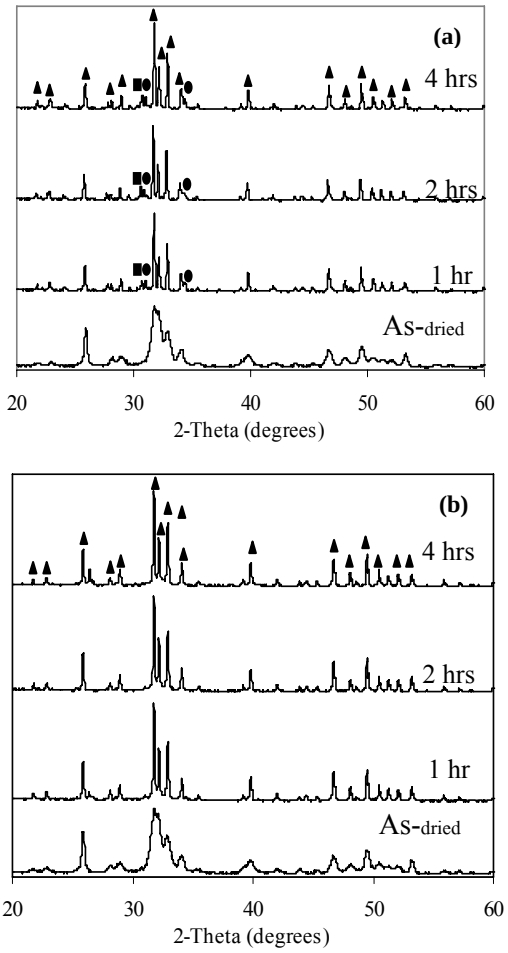

Figure 3. XRD Patterns of sintered HAW samples at (a) 1200°C and (b) 1250°C for 1 hour, 2 hours and 4 hours, ▲:HA, ●:β-TCP, ■:α-TCP.

The XRD patterns of the HAD samples sintered at 1200°C and 1250°C for 1, 2 and 4 hours are presented in Figure 4(a) and (b). With increased sintering time, the intensity of HA peaks was also not noticeably increased, which corresponds to HAW powder. Only the peaks depending on the β-TCP appeared as a minor phase after sintering at 1200°C and 1250°C for all sintering times. Wang et al. (1998) reported that sintered HA can lead to the partial thermal decomposition of HA into TCP and/or tetracalcium phosphate (TTCP). Thermal decomposition is composed of two steps i.e. dehydroxylation and decomposition. Dehydroxylation to oxyhydroxyapatite occurs at a temperature around 850-900°C by completely reversible reaction in accordance with Equation (1)[22]

$$Ca_{10}(PO_4)_6(OH)_2 \rightarrow Ca_{10}(PO_4)_6(OH)_{2-2x}O_x + xH_2O_{gas} \quad (1)$$

Upon sintering at higher temperatures (higher than 900°C), HA can decompose into TCP and TTCP in relation to Equation (2)[22].

$$Ca_{10}(PO_4)_6(OH)_2 \rightarrow 2Ca_3(PO_4)_2 + Ca_4P_2O_9 + H_2O_{gas} \quad (2)$$

However, the secondary phase from decomposition can be eliminated by controlling moisture content in the sintering atmosphere.[23] Hence, the appearance of β-TCP in HAD implies that the thermal stability of hydroxyapatite prepared by the solid-state reaction method is lower than that of hydroxyapatite produced by wet chemical precipitation route. In order to use hydroxyapatite as a bone substitution, the presence of β-TCP with small amount would be useful for speedy bonding of synthetic bones to natural ones throughout fast dissolution(Sung et al., 2004) but it can also impair the mechanical properties of HA ceramics.[25-26]

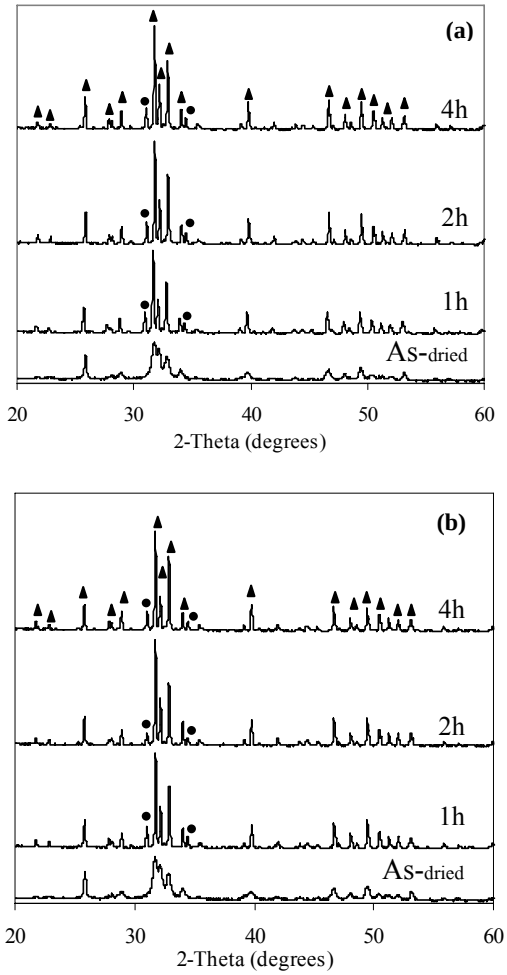

Figure 4. XRD Patterns of sintered HAD samples at (a) 1200°C and (b) 1250°C for 1 hour, 2 hours and 4 hours, ▲:HA, ●:β-TCP, ■:α-TCP.

Effect of Sintering Temperature and Time on Morphology of Sintered Samples

The SEM investigation of HAW samples sintered at 1200°C for 1, 2 and 4 hours is shown in

Figure 5. The microstructure was accompanied by the small pores that are constantly present on grain boundaries and are surrounded by several grains in the vicinity as illustrated in the low magnification images. Surprisingly, with increasing both sintering temperatures and times, no significant trend of increase of the average grain size was observed. Similarly, Figure 6 presents the SEM images of HAW samples sintered at 1250°C with various times. The microstructure illustrates an analogous morphology to the samples sintered at 1200°C. Therefore, the morphology of HAW samples might not have been influenced by the sintering temperatures and times in this study. This might be because there is little difference in sintering temperatures between 1200°C and 1250°C, so that the effect of sintering temperature on morphology could not be clearly seen.

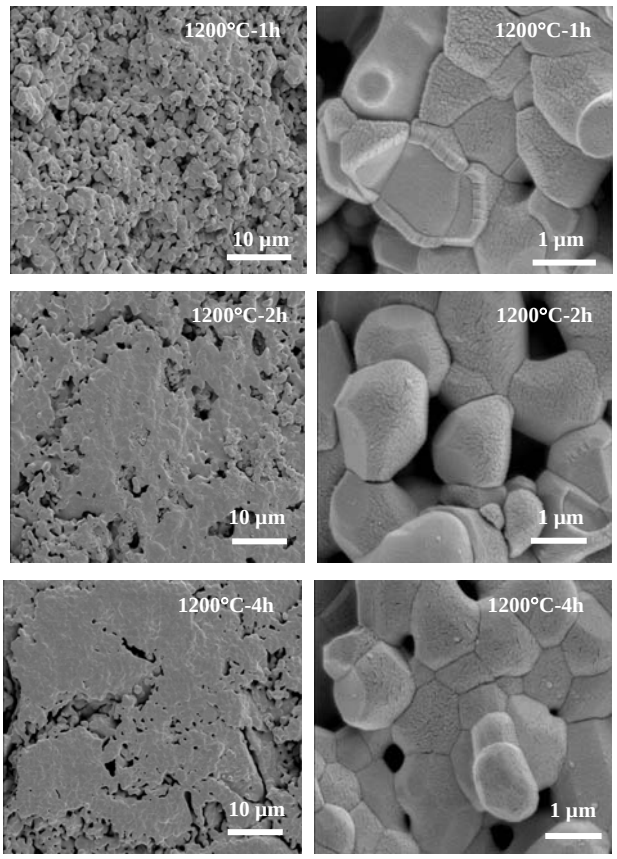

Figure 5. SEM images of sintered HAW samples at 1200°C for 1 hour, 2 hours and 4 hours with low and high magnifications.

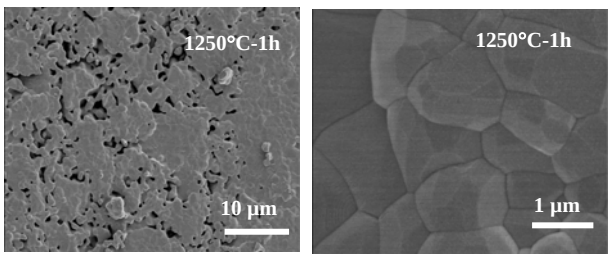

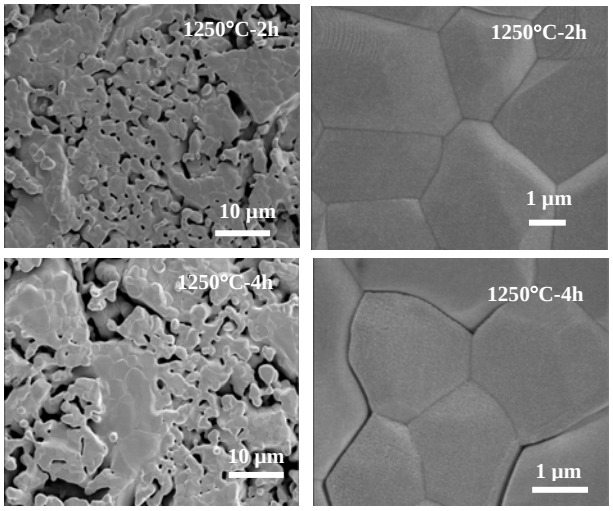

Figure 6. SEM images of sintered HAW samples at 1250°C for 1 hour, 2 hours and 4 hours with low and high magnifications.

The microstructure of HAD also consisted of tiny pores which always exist on grain boundaries and are enclosed by several grains in the vicinity as presented in Figures 7 and 8. The average grain sizes of the sintered samples at 1200°C and 1250°C were also not noticeable larger when the sintering time increased as reported in Table 1.

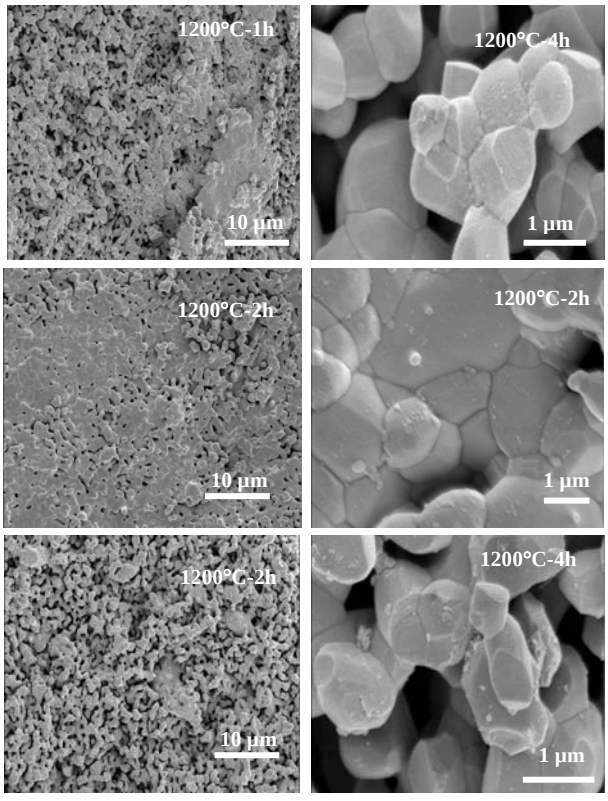

Figure 7. SEM images of sintered HAD samples at 1200°C for 1 hour, 2 hours and 4 hours with low and high magnifications.

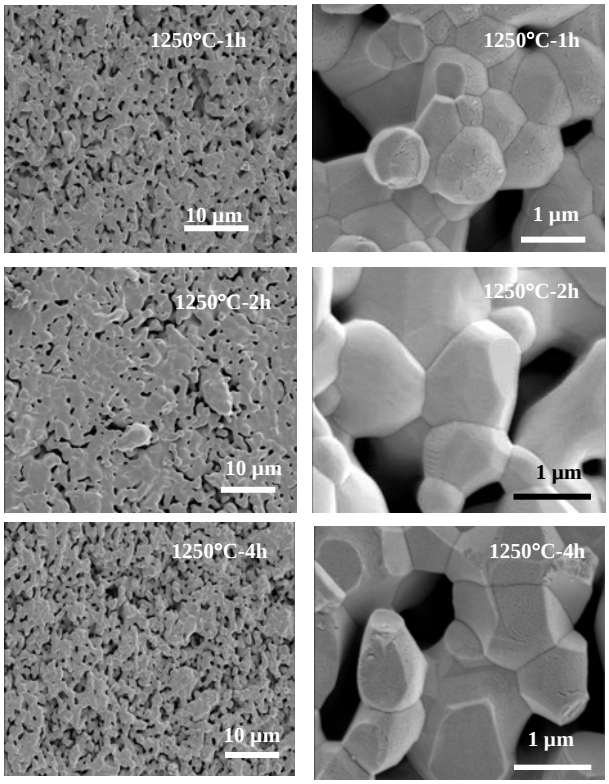

Figure 8. SEM images of sintered HAD samples at 1250°C for 1 hour, 2 hours and 4 hours with low and high magnifications.

Table 1. Summary of average grain sizes for all sintered samples.

Temp-time	Number of tests (grains)	Mean Grain size (µm)	Standard deviation (µm)
HAW 1200°C-1h	180	1.29	±0.43
HAW 1200°C-2h	180	1.62	±0.48
HAW 1200°C-4h	180	1.70	±0.50
HAW 1250°C-1h	180	1.32	±0.39
HAW 1250°C-2h	180	1.77	±0.64
HAW 1250°C-4h	180	2.54	±1.13
HAD 1200°C-1h	180	1.14	±0.34
HAD 1200°C-2h	180	1.62	±0.48
HAD 1200°C-4h	180	1.72	±0.43
HAD 1250°C-1h	180	1.50	±0.41
HAD 1250°C-2h	180	1.76	±0.63
HAD 1250°C-4h	180	2.08	±0.60

When comparing the grain sizes of sintered HAW and HAD samples, no obvious trend of grain size variation can be observed between different synthesizing methods when sintered at the same temperature and time. Liu (1997) suggested that smaller pore sizes exhibit a higher strength, so that both the mean grain size and the pore size exert influence on the mechanical strength of sintered HA samples. Consequently, it is important to balance between the pore size and the grain size to achieve the ultimate mechanical strength of the sintered bodies.[28]

Effect of Sintering Temperature and Time on Density and Porosity of Sintered Samples

Table 2 reports the bulk density and apparent porosity of all sintered samples. In HAW, the green density was 1.263 g/cm^3. It increased after sintering, and reached the maximum density at 2.621 g/cm^3, when sintering at 1250°C for 4 hours.

In HAD, the density had been raised with increasing sintering temperatures and times. It reached the maximum density at 2.223 g/cm^3, when sintering at 1250°C for 2 hours. Due to the large amount of water lost by decomposition of HA following Equation (2) created many pores in sintering disks resulting in the lower density. Therefore, the porosity of HAD samples was observed. This could explain the phenomenon of the lower density of HAD samples compared to that of HAW sintered samples as presented in Table 2.

Table 2. Bulk density and apparent porosity values of all sintered samples.

Temp-time	Bulk density (g/cm^3) ± SD.	Apparent porosity (%)
HAW 1200°C-1h	2.279±0.099	25.20
HAW 1200°C-2h	2.384±0.011	23.45
HAW 1200°C-4h	2.347±0.015	23.84
HAW 1250°C-1h	2.497±0.041	24.03
HAW 1250°C-2h	2.619±0.050	25.44
HAW 1250°C-4h	2.621±0.056	24.92
HAD 1200°C-1h	1.644±0.006	46.68
HAD 1200°C-2h	1.699±0.008	45.06
HAD 1200°C-4h	1.770±0.009	42.64
HAD 1250°C-1h	1.923±0.022	37.59
HAD 1250°C-2h	2.223±0.034	28.21
HAD 1250°C-4h	2.059±0.024	33.29

Effect of Sintering Temperature and Time on Flexural Strength of Sintered Samples

The influence of sintering temperature and time on flexural strength of sintered HAW and HAD at temperatures of 1200°C and 1250°C are reported in Table 3. In HAW, the strength was increased with increasing sintering temperature and time except for the sample sintered at 1200°C for 4 hours. This could be explained by the highest grain size with the combination phases of HA and TCP in this sample. As earlier mentioned, TCP

might debase the mechanical properties of the samples. However, this phenomenon has not been observed in HAW sintering at 1250°C for 4 hours because these samples contained the single phase of HA even though they obtained larger grain sizes than the sample sintered at 1200°C for 4 hours.

Table 3. Bending strengths of all sintered samples.

Temp-time	Number of tests	Mean bending strength (MPa)	Standard deviation (MPa)
HAW 1200°C-1h	5	19.87	±2.55
HAW 1200°C-2h	5	20.84	±6.86
HAW 1200°C-4h	5	12.32	±0.95
HAW 1250°C-1h	5	34.49	±3.36
HAW 1250°C-2h	5	37.20	±5.90
HAW 1250°C-4h	5	42.73	±7.53
HAD 1200°C-1h	5	10.55	±1.77
HAD 1200°C-2h	5	12.58	±2.05
HAD 1200°C-4h	5	12.88	±2.33
HAD 1250°C-1h	5	24.30	±8.18
HAD 1250°C-2h	5	40.35	±8.67
HAD 1250°C-4h	5	30.41	±6.07

In contrast to HAW, a decrease of strength was observed in HAD sample after sintering at 1250°C for 4 hours, but not in samples sintered at 1200°C for 4 hours. This is a result of the larger grain size of samples sintered at 1250°C for 4 hours in comparison with samples sintered at 1200°C for 4 hours although both HA and TCP can be indexed in these samples. Consequently, it can be concluded that the finer grain size is the reason for the higher the flexural strength of the samples.

In densification process, therefore, sintering temperature has a more crucial effect than sintering time on average grain and pore sizes, density and mechanical properties of sintered samples. Even though sintering time exerts a less significant role on properties of HA, choosing the correct sintering time must be carried out very carefully due to fact that the unsuitable sintering profile could cause a decrease in density and strength of sintered specimens. Therefore, the appropriate sintering schedule for HA powder from different synthesizing methods is essential. Not only does the sintering schedule need to be considered, but the pressing process and firing atmosphere are also important to achieve the maximum mechanical properties. Additional work is being conducted in order to improve physical and mechanical properties in synthesized HA.

Conclusions

Nano-sized HA powders were synthesized by wet chemical and solid-state reaction methods with different particle sizes and specific surface area. After sintering, bulk density and flexural strength increased with increasing sintering temperature except. Nonetheless, this did not apply to grain sizes. It seems that the sintering temperature had a more pronounced effect rather than the sintering time as no radical trends of increase in grain size, density and strength could be observed with increasing sintering time. In addition, the decomposition of β-TCP and α-TCP resulted in lower thermal stability in sintered HAD, causing lower density and weaker fracture strength compared to HAW. Therefore, morphology and properties of sintered HA can be controlled by variation of particle size, which was prepared by different powder preparation routes together with the suitable sintering schedule.

Acknowledgements

The authors acknowledge the financial support given by the National Metal and Materials Technology Center, the Ministry of Science and Technology of Thailand, under Project No. MT-B-50-BMD-07-131.

References

1. Hench, L.L. (1991). Bioceramics: from concept to clinic. *J. Am. Ceram. Soc.* **74**: 1487-1510.

2. LeGeros, R.Z. & Legeros, J.P. (1993). Dense hydroxyapatite. In : L.L. Hench & J. Willson (eds.). *An introduction to bioceramics*. London: World Scientific: pp. 139-180.

3. Tracy, B.M. & Doremus, R.H. (1984). Direct electron microscopy studies of the bone-hydroxyapatite interface. *J. Biomed. Mater. Res*. **18(7)** : 719-726.

4. Jarcho, M., Bolen,C.H., Thomas, M.B., Bobick, J., Kay, J.F. & Doremus, K.H. (1976). Hydroxyapatite synthesis and characterization in dense polycrystalline form. *J. Mater. Sci.* **11**: 2027-2035.

5. Liu, C., Huang, Y., Shen, W. & Cui, J. (2001). Kinetics of hydroxyapatite precipitation at pH 10 to 11. *Biomaterials* **22(4)** : 301-306.

6. Santos, M.H., de Oliveira, M., de Freitas Zouza, L.P., Mansur, H.S. & Vasconcelos, W.L. (2004). Synthesis control and characterization of hydroxyapatite prepared by wet precipitation process. *Mater. Res.* **7(4)** : 625-630.

7. Zhang, S. & Gonsalves, K.E. (1997). Preparation and characterization of thermally stable nanohydroxyapatite. *J. Mater. Sci.: Mater. Med*. **8(1)** : 25-28.

8. Afshar, A., Ghorbani, M., Ehsani, N., Saeri, M.R. & Sorrel, C.C. (2003). Some important factors in the wet precipitation process of hydroxyapatite. *Mater. Design.* **24(3)** : 197-202.

9. García, C., Paucer, C., Gaviria, J. & Duran, A. (2005). Effect of some physical-chemical variables in the synthesis of hydroxyapatite by the precipitation route. *Key Eng. Mater.* **284-286**: 47-50.

10. Arita, I.H., Castano, V.M. & Wilkinson, D.S. (1995). Synthesis and processing of hydroxyapatite ceramic tapes with controlled porosity. J. *Mater. Sci.: Mater. Med.* **6(1)** : 19-23.

11. Kim, W., Zhang, Q. & Saito, F. (2000). Mechanochemical synthesis of hydroxyapatite from $Ca(OH)_2$-P_2O_5 and CaO-$Ca(OH)_2$-P_2O_5 mixtures. *J. Mater. Sci.* **35(21)** : 5401-5405.

12. Zhang, X. & Vecchio, K.S. (2007). Hydrothermal synthesis of hydroxyapatite rods. *J. Cryt. Growth*. **308(1)** : 133-140.

13. Zhu, R., Yu, R., Yao, J., Wang, D. & Ke, J. (2008). Morphology control of hydroxyapatite through hydrothermal process. *J. Alloy Comp.* **457(1-2)**: 555-559.

14. Kothapalli, C., Wei, M., Vasiliev, A. & Shaw, M.T. (2004). Influence of temperature and concentration on the sintering behavior and mechanical properties of hydroxyapatite. *Acta Materialia*. **52(19)** : 5655-5663.

15. Webster, T.J., Ergun, C., Doremus, R.H., Siegel, R.W. & Bizios, R. (2001). Enhanced osteoclast-like cell functions on nano-phase ceramics. *Biomaterials*. **22(11)** : 1327-1333.

16. Cao, L.Y., Zhang, C.B. & Huang, J.F. (2005). Synthesis of hydroxyapatite nanoparticles in ultrasonic precipitation. *Ceram. Int.* **31(8)**: 1041-1044.

17. Kong, L.B., Ma, J. & Boey, F. (2002). Nanosized hydroxyapatite powders derived from coprecipitation process. *J. Mater. Sci.* **37(6)** : 1131-1134.

18. Akao, M., Aoki, H. & Kato, K. (1981). Mechanical properties of sintered hydroxyapatite for prosthetic applications. *J. Mater. Sci.* **16(3)** : 809-812.

19. Martin, R.I. & Brown, P.W. (1995). Mechanical properties of hydroxyapatite formed at physiological temperature. *J. Mater. Sci.: Mater. Med.* **6(3)** : 138-143.

20. Somiya, S. (1989). Advanced technical ceramics. California : Academic press: pp. 230-231.

21. Rodriguez-Lorenzo, L.M., Vallet-Regi, M. & Ferreira, J.M.F. (2001). Colloidal processing of hydroxyapatite. *Biomaterials*. **22(13)** : 1847-1852.

22. Wang, C.K., Ju, C.P. & Lin, J.H.C. (1998). Effect of doped bioactive glass on structure and properties of sintered hydroxyapatite. *Mater. Chem. Phys.* **53(2)** : 138-149.

23 Sadeghian, Z., Heinrich, J.G. & Moztarzadeh, F. (2006). Influence of powder pre-treatments and milling on dispersion ability of aqueous hydroxyapatite-based suspensions. *Ceram. Int.* **32(3)** : 331-337.

24. Sung, Y.M., Lee, J.C. & Yang, J.W. (2004). Crystallization and sintering characteristics of chemically precipitated hydroxyapatite nanopowder. *J. Cryt. Growth*. **262(1-4)** : 467-472.

25. Royer, A., Viguie, J.C., Heughebaert, M. & Heughebaert, J.C. (1993). Stoichiometry of hydroxyapatite: Influence on the flexural strength. *J. Mater. Sci.: Mater. Med.* **4(1)** : 76-82.

26. Wang, P.E. & Chaki, T.K. (1993). Sintering behavior and mechanical properties of hydroxyapatites and dicalcium phosphate. *J. Mater. Sci.: Mater. Med.* **4(2)** : 150-158.

27. Liu, D.M. (1997). Influence of porosity and pore size on the compressive strength of porous hydroxyapatite ceramic. *Ceram. Int.* **23(2)** : 135-139.

28. Rodríguez-Lorenzo, L.M., Vallet-Regí, M. & Ferreira, J.M.F. (2001). Fabrication of hydroxyapatite bodies by uniaxial pressing from a precipitated powder. *Biomaterials*. **22(6)** : 583-588.